Coarse root distribution of a semi-arid oak savanna estimated with ground penetrating radar

Naama Raz-Yaseef,[1] Laura Koteen,[1] and Dennis D. Baldocchi[1]

Received 24 August 2012; revised 15 November 2012; accepted 17 November 2012; published 11 February 2013.

[1] The binary nature of Northern California's ecohydrology, in which water is either abundantly available or scarce, should be reflected in the root architecture of the native blue oak. Our objective was to quantify carbon storage and understand how the form of the root system facilitates ecosystem functioning despite the asynchrony between winter water availability, spring leaf growth, and dry-summer canopy maintenance. To do this, we surveyed coarse root distribution with a ground penetrating radar (GPR), due to its advantages in covering large areas rapidly and non-destructively. We calibrated root biomass detected by GPR against roots excavated from a number of small pits. Based on a survey of six tree configurations (varying in age, size, and clumping), we found that coarse roots occupy the full soil profile and that coarse root biomass of old large trees reached a peak directly above the bedrock. As opposed to other semi-arid regions, where trees often develop extensive shallow lateral coarse roots to exploit the entire wet-soil medium, we found that root density decreased with distance from the bole, and dropped sharply beyond a distance of 2 m. We upscaled tree root biomass to stand scale ($2.8 \pm 0.4\,kg\,m^{-2}$) based on lidar analysis of the relative abundance of each tree configuration. We argue that this deep and narrow root structure reflects the ecohydrology of oaks in this ecosystem. An extensive lateral root system would not be beneficial during the growing season, when water is sufficiently abundant, nor during summer, when soil water is highly limited.

Citation: Raz-Yaseef, N., L. Koteen, and D. D. Baldocchi (2013), Coarse root distribution of a semi-arid oak savanna estimated with ground penetrating radar, *J. Geophys. Res. Biogeosci.*, *118*, 135–147, doi:10.1029/2012JG002160.

1. Introduction

[2] Tree roots play a critical role in a wide range of ecosystem processes and feedbacks but remain poorly quantified compared to aboveground structure and function. In woody vegetation, functional roles are divided between fine and coarse roots: nutrients, oxygen, and water are obtained by fine roots and their associated mycorrhizae, and coarse roots support the network of fine roots, deliver nutrients and water to the shoots, and support the tree structure *Fogel*, 1983. Fine roots track changes in aboveground phenology, and in soil temperature, moisture and nutrient availability [*Cheng and Bledsoe*, 2002], resulting in seasonal changes in biomass and distribution, and high annual turnover rates [*Day et al*., 1996]. Although fine root production on an annual basis is generally high, their contribution to the total belowground biomass is comparatively small [*Vogt et al*., 1996]. Coarse roots, oppositely, grow at a rate similar to that of aboveground biomass, such that their size is closely correlated to tree size and age [*Velten and Richter*, 1995; *Millikin and Bledsoe*, 1999; *Makela et al*., 2008]. Biomass ratios between roots and shoots in trees maintain a balance between carbon allocation to aboveground growth, which increases plant photosynthetic and reproductive capacity, and carbon allocation to belowground growth, which increases access to soil water and nutrients [*Lynch*, 1995; *Kleidon and Heimann*, 1998]. The stability of the root-shoot ratio allows one to calculate belowground biomass relatively accurately based on allometric relationships with tree width and height [*Drexhage et al*., 1999]. Information on root biomass is important for determining the size of carbon pools and fluxes. But in order to upscale root biomass, identify water sources, and estimate tree sensitivity to climatic and landscape changes, additional information on the spatial distribution of roots is essential. Yet, such information is often unavailable.

[3] In general, root distribution follows some broad consistent patterns and tracks resource availability in space and time. In most ecosystems, the majority of roots are found in the upper 30 cm of the soil, and root density decreases with increasing distance from the bole [*Stone and Kalisz*, 1991; *Canadell et al*., 1996; *Jackson et al*., 1996; *Schenk and Jackson*, 2002]. The tendency of roots to proliferate around the bole is self-perpetuating, because the mineralization of essential nutrients for future root acquisition is, in part, supplied by microbial decomposition of existing roots. In addition, soil moisture is often higher near the bole, because

[1]Department of Environmental Science, Policy and Management, University of California, Berkeley, California, USA.

Corresponding Author: N. Raz-Yaseef, Department of Environmental Science, Policy and Management, University of California, Berkeley, 105 Hilgard Hall, Berkeley, CA 94720, USA. (RYNaama@gmail.com)

2169-8953/13/2012JG002160

tree canopies reduce rainfall intensity, the presence of plant litter reduces runoff, roots improve infiltration processes, organic material increases soil water holding capacity, and tree shading and plant litter slow soil evaporation. But root systems do not look like upside down tree canopies; root distribution varies considerably across space and time, making it even more challenging to study these buried systems. Additional factors that contribute to root distribution patterns may be more site specific and include characteristics such as soil depth, texture, salinity, nutrient availability, water holding capacity, and root competition from other community dominants [*Kramer*, 1969; *Coomes and Grubb*, 2000; *Yanai et al*., 2006; *Macinnis-Ng et al*., 2010]. Climate also has a major effect on root distribution, especially in ecosystems where water is limited. Root systems tend to be shallow and laterally extensive in semi-arid climates [*Jackson et al*., 1996; *Vogt et al*., 1996; *Schenk and Jackson*, 2002; *Guswa*, 2008], in response to the short and sporadic nature of precipitation, which limits soil water infiltration to shallow depths [*Sala et al*., 1982]. In arid ecosystems, roots tend to explore deeper layers for water pools. In addition to groundwater, moisture stored in bedrock and in deep soil layers can play an important role in the survival of vegetation in semi-arid climates [*Heisler-White et al*., 2008; *Knapp et al*., 2008; *Schwinning*, 2010; *Yaseef et al*., 2010]. Nonetheless, plants tend to grow roots only to depths that are sufficient for the provision of resource requirements and are constrained by the imperative to reduce maintenance costs during periods of stress [*Schenk and Jackson*, 2002].

[4] The oak-grass savanna vegetation at our research site is typical of large areas in Northern California [*Tyler et al*., 2006; *Baldocchi et al*., 2010]. This region enjoys wet and mild winters but experiences extreme hot, dry summer conditions, with occasional drought years. The understory is dominated by cool-season C_3 annual species, but the overstory oaks are winter decidous, despite the severity of summer conditions. Oak leaf growth begins in early spring, when temperatures are moderate and soil water is ample, and a full canopy is maintained throughout the dry summer and until the onset of the next cool season in autumn. In that sense, trees are out of synchrony with water availability but benefit from the greater warmth and extended photoperiod of spring and summer. Water uptake from groundwater helps explain the incongruity of tree growth with soil water availability in this ecosystem. Roots growing in bedrock cracks are observed at open cleavages in this region, and evidence for groundwater uptake by blue oaks was obtained by tracer studies for a nearby site [*Lewis and Burgy*, 1964]. At our site, the high correlation between fluctuations in groundwater depth and sap flux measurements indicates that tree water uptake from groundwater accounts for up to 80% of the evapotranspiration flux during the dry summer months [*Miller et al*., 2010].

[5] We sought to characterize root architecture and to integrate root function into an emerging picture of ecosystem pattern and process at a site for which there is an extensive measurement record of carbon and water exchange and a comprehensive set of aboveground measurements. Our specific objectives were (1) to define tree level coarse root biomass and test the potential for upscaling based on lidar measurements of aboveground canopy structure in order to estimate stand level carbon storage, (2) to understand coarse root structure in order to explain how root architecture in this Mediterranean-type oak-savanna ecosystem is capable of supporting aboveground demands for water and nutrients during both the short wet spring and the long dry summer seasons, and (3) to examine the applicability of ground penetrating radar, as described below, in surveying coarse roots.

2. Materials and Methods

2.1. Applicability of Ground Penetrating Radar (GPR) for Surveying Coarse Roots

[6] Standard methods to investigate root architecture include sampling by means of trenches, pits, and cores [*Thomas and Hartmann*, 1998; *Park et al*., 2007; *Macinnis-Ng et al*., 2010], as well as excavation of the entire root systems [*Drexhage et al*., 1999]. These methods are laborious and costly and can be destructive to trees, often necessitating small sample sizes. Recently, use of ground penetrating radar (GPR) to map and quantify whole tree root systems in situ has been tested and applied to a range of ecosystems [*Hruska et al*., 1999; *Butnor et al*., 2001; *Barton and Montagu*, 2004; *Stover et al*., 2007; *Dannoura et al*., 2008; *Zenone et al*., 2008]. The application of this method is promising, because it is non-destructive, rapid, comparatively low cost, and can be applied to relatively large areas, giving a more complete picture of root architecture at the landscape scale.

[7] GPR has long been applied to detect structures and features buried in the ground. The first report of GPR usage was that given by *Stern* [1929], who used it to estimate the extent of a glacier in Austria. Since then, GPR has been deployed on space shuttles, airplanes, inside boreholes, and on the surface of the moon [*Olhoeft*, 2002]. Currently, GPR is routinely used in commercial applications, as a tool to locate pipes and cables within the upper 2 m below the surface. GPR are also used as a geophysical research tool, and some examples of applications are detection of archeological sites [*Pérez Gracia et al*., 2000], caves and mines [*Chamberlain et al*., 2000], burials [*Schultz et al*., 2006] and fossils, sedimentary processes, rock fractures and fissures [*Adrian*, 2004], soil water content measurements [*Grote et al*., 2003; *Huisman et al*., 2003], groundwater dynamics [*Yoshikawa and Hinzman*, 2003], ice sheet and permafrost [*Vaughan et al*., 1999], and forestry applications [*Lorenzo et al*., 2010]. While roots are considered as an unwanted source of noise in these applications, GPR can also be used to specifically detect coarse tree roots.

[8] Ground penetrating radar is based on the observation that materials differ in their dielectric capacity. The dielectric permittivity of a material expresses the ability to decrease the attraction between electrical particles, as a function of the electric displacement and intensity of an electrical field. The permittivity of materials is measured relative to that of air, such that the dielectric constant of air = 1 and that of dry wood = 1.4. Soil minerals are in the range of 3–10, and the permittivity of water is significantly different: 78.5 at 25 °C [*Jones et al*., 2002; *Robinson et al*., 2003]. The high permittivity of water originates in the polarization of the water molecule; when placed in an electrical field, a water molecule will align with the field, enabling it to store energy and react as a dielectricum. Soils are a mixed medium of varying amounts of minerals, organic material, gas, and

water, but their dielectric constant will be mostly determined by water content.

[9] When a traveling electromagnetic wave hits a boundary between materials with different dielectric constants, such as a dry soil and a water-conducting root, part of it will be reflected. The reflected fraction is proportional to the difference in the dielectric permittivity between the materials. The difference in dielectric permittivity of a root and its surrounding matrix, and therefore the ability of a traveling electromagnetic wave to detect this boundary, varies in time and space as a function of soil characteristics (texture, water content) and root characteristics (size, depth, orientation, water content) [*Zanetti et al*., 2010].

[10] Ground penetrating radar is comprised of two major components: a radio-wave emitter and a receiver antenna that picks up the electromagnetic returning signal [*Daniels*, 1996]. The depth of the buried objects is defined by GPR according to the wave travel time (emitter to the receiver). When a GPR is carried over a surface, it generates successive pulses, resulting in a pseudo-image in the form of a hyperbola, with the vertex located above the shortest distance to the object (Figure 1). In a typical GPR profile (Figure 2), the direction of progress is presented as distance on the horizontal axis, and time duration (equivalent to depth) of the returning pulse is in the vertical direction.

[11] GPR surveys to study tree roots began more than a decade ago [*Hruska et al*., 1999]. Since then, GPR methodology has been improved and refined, based on various field observations [*Butnor et al*., 2001; *Butnor*, 2003; *Barton and Montagu*, 2004; *Zenone et al*., 2008], controlled experiments with buried roots [*Dannoura et al*., 2008; *Hirano et al*., 2008], and used in a number of environmental studies [*Fourcaud et al*., 2002; *Cox et al*., 2005; *Stover et al*., 2007]. In the following paragraph, we summarize issues that have arisen in previous studies which require consideration when surveying tree roots with GPR.

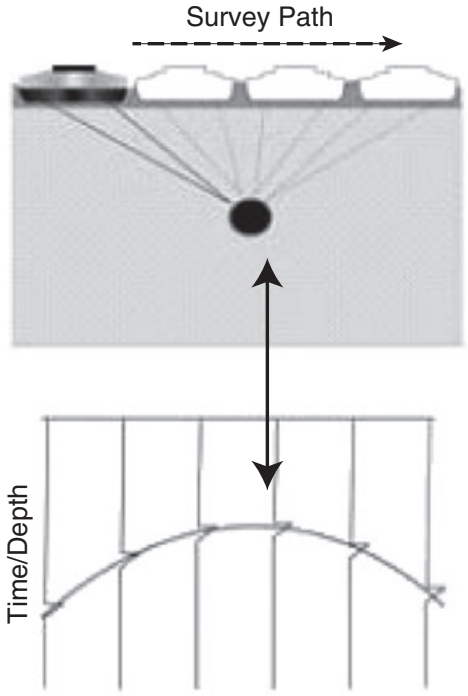

Figure 1. Schematic representation of a GPR passing along the ground surface above a buried object (upper pane) and the obtained pseudo-image (lower pane). Because electromagnetic waves are sent and received in all directions, the reflections produce a hyperbola with the vertex above the position where the approach to the object is shortest.

[12] The first concern relates to site compatibility. Ideally, the site should have a flat terrain, with limited or low density herbaceous understory vegetation, to allow ease of access and continuous measurements. In soils, energy is absorbed and scattered by water, salts, and clay particles; therefore, ideally these attributes should be low, to achieve good root representation. For example, *Butnor et al*. [2001] showed that penetration depths with a 400 MHz GPR were reduced from 5 m in a sandy soil, to less than 2 m in a clayey soil. Bedrock, which borders the GPR root-detection horizon, and the existence of small rocks inside the soil, which can be mistaken for roots, are also important factors to be considered. The second concern relates to the selection of radar frequency, which should account for tradeoffs between penetration depth and image resolution. High-frequency waves quickly dissipate in the ground, and an electromagnetic wave of 2 GHz will usually penetrate only to a depth of 20 cm, while a 100 MHz wave can penetrate up to 30 m. However, a decrease in frequency will result in a loss of resolution; higher frequencies produce a smaller, more focused antenna footprint. High resolution is important for the detection of small objects such as roots, and will also allow to differentiate between adjacent roots. Previous research has shown that for the application of coarse root detection (for practical reasons, fine and coarse roots are often separated based on a diameter threshold of 2 mm [*Bohm*, 1979]), GPR frequencies within the range of 400 MHz and 1.5 GHz are most effective [*Butnor et al*., 2001; *Barton and Montagu*, 2004; *Zenone et al*., 2008]. A frequency of 1 GHz such as the one used in this study has a typical resolution of 1 cm. Lastly, there is a need to determine the optimal time period to perform GPR measurements. A clear signal from the root/soil interface can be expected when the difference between the water content within the root and the soil is largest [*Hirano et al*., 2008; *Zenone et al*., 2008]. *Dannoura et al*. [2008] showed that roots were not detectable when soils were wetter than roots; even under more ideal conditions, not all roots with water content $< 25\%$ could be detected.

[13] While all quoted studies found GPR technology adequate and successful in quantifying coarse tree roots, they also reported on the need to further improve signal processing and to better define the effect of site conditions on GPR readings. Because GPR remains a relatively new technology for examining root structure, an ancillary objective of our research was to test this methodology and help facilitate its application more broadly.

2.2. Field Site

[14] The research site is located in Northern California, USA, on the foothills of the Sierra Nevada Mountains near Sacramento (38°43′N and −120°97′E). The terrain is predominantly flat, at a height of 177 above sea level. Soils are shallow, typically not deeper than 40 cm, of silt-loam texture, classified as Auburn-Exchequer. The underlying

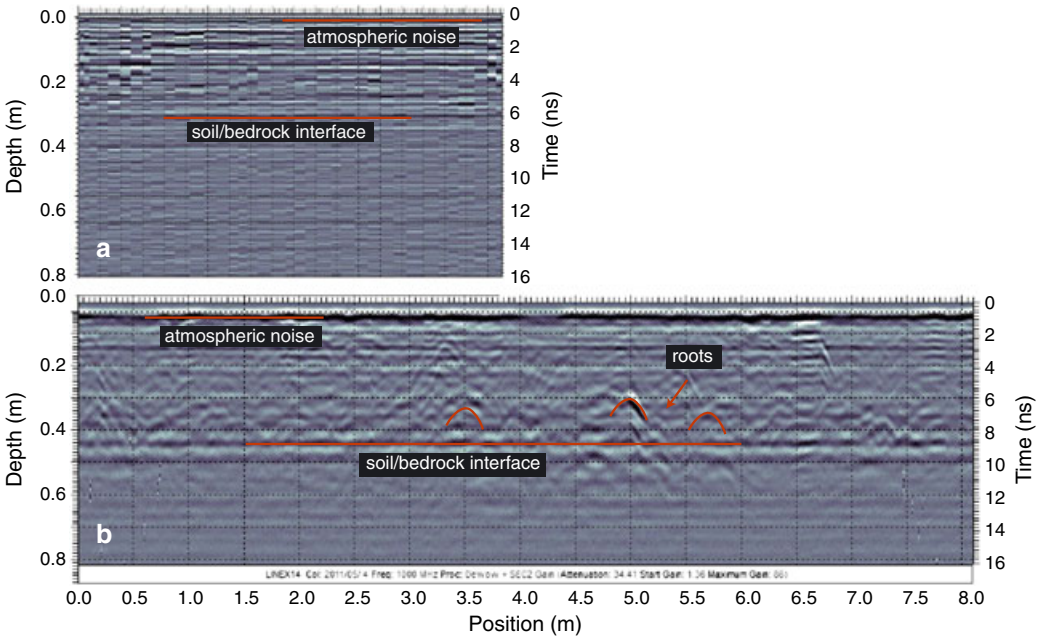

Figure 2. Depth profiles of GPR reflections for two surveyed lines: over an area remote from trees (a) and an area below a tree canopy (b). The *x* axis is distance (m) along the established grid, and the *y* axis is travel time (ns), which correlates to soil depth (m). The continuous line at approximately 0.30 m in Figure 2a and 0.45 m in Figure 2b was verified as bedrock in the excavated pits. Noise created by atmospheric interference at the upper part of the profile was stronger below the canopy. In Figure 2b, hyperbola-shaped reflections were later verified in situ as coarse tree roots (some are highlighted with red).

bedrock is comprised of slate and schist. Mean annual temperature for the site is 16.5 ± 0.7 °C, and mean annual precipitation is 562 ± 193 mm. The climate is Mediterranean, characterized by high seasonality, with moderately cool and wet winters and hot and dry summers (Figure 3). Groundwater table depth ranges between 10.5 m below the surface (December–January) to 9.5–8 m (April–May). Following years with a thick snow cover over the Sierra Nevada, spring groundwater depth as shallow as 3 m has been measured.

[15] The ecosystem is comprised of an oak-grass savanna, which is characteristic for this region. Vegetation phenology tracks site seasonality, with the grass understory and oaks each responding to unique environmental cues. With the onset of rains in late autumn, the annual grasses germinate and grow. Over the same period, the trees are dormant and leafless, and remain so throughout the cool winter. By mid- to late spring, soils dry out and grasses reproduce and die off. Yet for trees, spring is the peak activity season. Trees leaf out and acquire woody biomass as temperatures rise, shifting increasingly towards a maintenance phase through the hot, dry summer months (Figure 3). The trees are predominantly blue oaks (*Quercus douglasii*), with occasional gray pines (*Pinus sabiniana*; 3 per hectare). The oaks were approximately 10 m tall, with a 6.5 m crown diameter, landscape LAI of 0.7, stem density of 144 ha^{-1}, and a 65% coverage of the landscape [*Baldocchi et al*., 2010]. The understory annual species include *Brachypodium distachyon*, *Avena spp*., and *Bromus hordeaceous*. Maximum (April) LAI of these grasses varies annually but ranges between 1 and 2. Annual average of net ecosystem exchange (NEE) for the tree overstory and grassland understory was -367 and 269 $gC\,m^{-2}\,yr^{-1}$, respectively [*Ma et al*., 2007].

[16] The GPR survey was conducted during late spring of 2011 (DOY 122–124), 5 weeks after a large rain event of 180 mm, so that soils were at the dry-down stage, but tree water uptake rates were still high. The hydrological year of 2010–2011 received 577 mm of total precipitation, similar to the long-term average at the site. Meteorological conditions during the 4-day survey period were relatively constant. Air temperature ranged between 10 °C at night and 31 °C at noon, relative humidity between 72% at night and 15% at noon, and daily maximum incoming net radiation was 755 $W\,m^{-2}$. Soil water content measured with TDRs' at the field site decreased rapidly during the short survey period, from 23% to 19% at a depth of 5 cm and from 22% to 20% at a depth of 50 cm. At the time of survey, trees had completed leaf growth, and ecosystem fluxes were near peak activity (GPP was 2.98 g C $m^{-2}\,d^{-1}$ and evapotranspiration was 1.46 mm H_2O d^{-1} on average for the survey period—overstory and understory combined). As described previously, these conditions were optimal for GPR detection of roots.

2.3. Measurement and Sampling Scheme

[17] The GPR survey was conducted at six tree locations of various size, age, and clumping. Each survey covered an area of 8×8 m or less, when limited by spatial constraints and bole position (Table 1). In order to best represent the diversity of tree size and age at the field site, we surveyed two large trees (Grid 3 and Grid 4), one small tree (Grid 5), one extremely large and old tree (Grid 7), and two tree clusters (Grid 2 and Grid 6). Cluster measurements were conducted around one central trunk, with additional 4–6 trees surrounding the surveyed area. This configuration captured the variability of trees of different size, age, and clumping

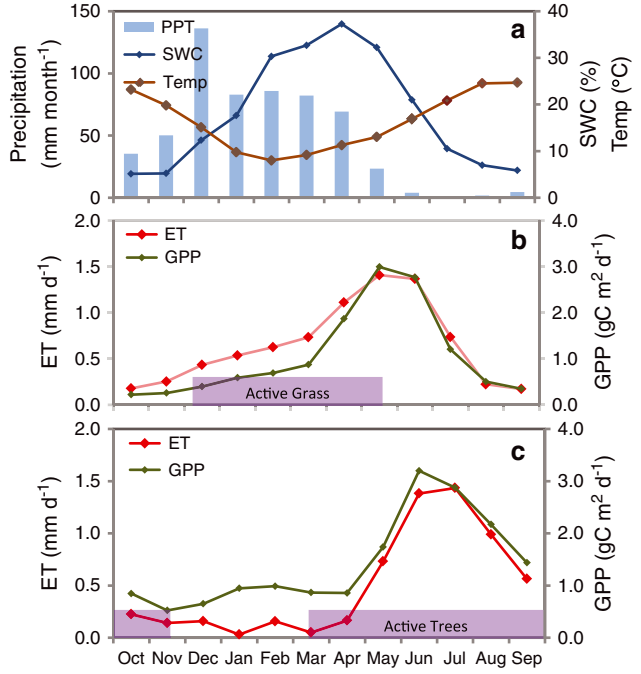

Figure 3. Annual trend of meteorological conditions and ecosystem fluxes at the research site. Values are monthly averages for the period October 2001–October 2011. (a) Precipitation (PPT; monthly sum), soil water content (SWC; monthly average), and air temperature (Temp; monthly average). (b) Gross primary production (GPP; daily average per month) and evapotranspiration (ET; daily average per month) measured over the forest floor (grass and soil). (c) The same as in Figure 3b but for fluxes measured above the canopy (trees). The phenologic active period of the grass and trees are noted. The grass is active during the main wet season, while the trees leaf out when temperatures rise, peak during late spring, and maintain fluxes during the entire dry summer.

at our field site, within the defined time and cost limits. Grass cover was relatively consistent within and between grids, with no visual differences across the landscape.

[18] In order to assess root biomass, we calibrated GPR signals against root biomass excavated from several pits. We positioned two rectangles of size 60 × 100 cm in each of the grids prior to GPR measurements, at distances of 0.50 and 1.50 m from the main bole (Figure 4). Following GPR measurements, each pit was dug down to bedrock.

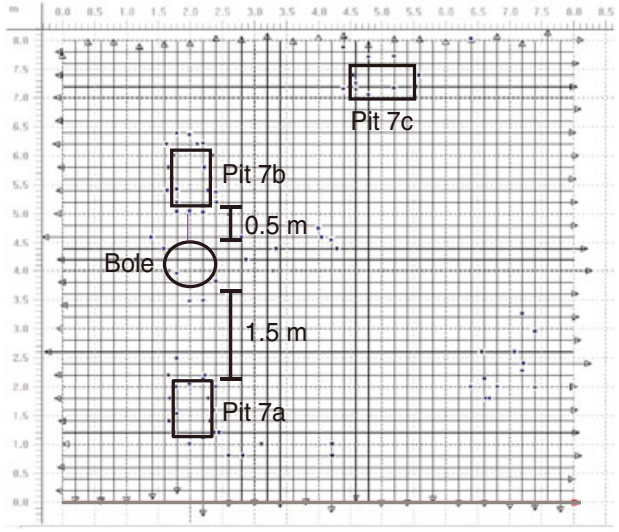

Figure 4. Surveyed X-Y lines collected for Grid 4. The location of two 60 × 100 cm pits, which were later excavated, and the position of the tree bole are shown. Black dots are fiducials marked during the GPR survey.

The excavated soil was sieved on site (mesh size of 2.25 × 2.25 cm, sieve size 0.9 × 0.9 m), and all visible roots >2 mm in diameter were harvested in regular depth intervals. To ensure that the great majority of roots were obtained, the excavated soil was sieved onto a tarp and sieved again by shoveling the soil and roots that fell through the mesh on the first pass back onto the sieve. In the lab, roots were washed of soil, sorted into size classes, dried, and weighed.

[19] We used a GPR Noggin1000 SmartTow (Sensors and Software Inc., Ontario, Canada) configuration, in which 1 GHz frequency radar was connected to a handle and to a large odometer wheel. The Noggin was attached to a battery and a digital video logger, on which real-time collected data were presented during data acquisition. GPR data were collected in perpendicular X-Y lines, to allow maximum coverage of the surveyed area. In each direction, parallel lines were equally spaced 20 cm apart, and marked with ropes, so that each 8 × 8 m grid contained 41 × 41 lines. Odometer calibration was verified prior to measurements. The spatial distance between observation points along each surveyed line (station interval) was set to 1 cm. Radar frequency of 1 GHz allowed for a detection resolution of approximately 1 cm. The survey was conducted at a slow, constant pace, first measuring all X

Table 1. Description of the Six Surveyed Tree Areas

	Grid 2	Grid 3	Grid 4	Grid 5	Grid 6	Grid 7	Average ± STD
Configuration	Cluster	Large tree	Large tree	Small tree	Cluster	Large, old tree	
Size (m × m)	8 × 4	8 × 8	8 × 8	8 × 8	8 × 7	8 × 8	
Tree height[a] (m)	11.5	12.9	10.4	6.0	11.7	9.8	10.4 ± 2.2
Tree dbh[a,b] (cm)	34	65	46	27	33	75	47 ± 19
Soil depth in pits (cm)	24, 25	46, 62	31, 48	14, 15	60, 65	35, 45, 50	40 ± 17
Soil depth, GPR[c] (cm)	33 ± 13	40 ± 16	39 ± 14	34 ± 15	34 ± 14	39 ± 16	37 ± 15
Total root biomass (kg)	174	592	478	260	350	521	396 ± 162
Total root biomass (kg m^{-2})	6.6	11.4	8.8	4.3	6.9	10.6	± 2.7

[a]For tree cluster, tree height and dbh is of the main, central tree.
[b]Diameter at breast height.
[c]GPR estimates, averaged for the whole grid.

direction lines and then measuring all Y direction lines. The locations of the bole (over which data were not collected) and pits were marked with fiducials (i.e., a reference point positioned in the field and observed in the produced image).

[20] GPR raw data were analyzed with designated software (GFP_Edit, EKKO_View, EKKO_Mapper; Sensors and Software Inc., Ontario, Canada). This included constructing grids from the collected lines according to the odometer readings and line numbers (Figure 4), performing a standard GPR processing routine (DME; Dewow, Migration and Enveloping), and defining signal velocity according to hyperbola shape. These procedures allowed to collapse hyperbolas into line segments and connect transects into a plan view. Thus, points of high contrast in dielectric conductivity, presumably representing a soil/root interface, were transformed into lineaments representing roots. We geo-positioning each grid with GPS readings from the corners of the grids in order to view them on an aerial view (Figure 5). Next, the three-dimensional values of radar reflection intensity were exported to MATLAB. Here a matrix with GPR values was prepared for each pit by extracting the corresponding area from the larger grid. We compared the two matching values for each of the 12 pits—GPR intensity and excavated root biomass—and used these data sets to obtain a calibration equation to convert GPR readings into root biomass. Subsequently, we analyzed the three-dimensional data to determine root distribution with depth and root distribution with distance from trees (rings of increasing radii extending from the bole to the largest perimeter entirely included within each grid).

[21] Upscaling root biomass from grid to stand scale was achieved by calculating the proportion of each measured tree configuration (size and clumping) in the oak-savanna woodland. We used an existing database of tree height and canopy width analyzed from airborne lidar data [*Chen et al*., 2008; *Kobayashi et al*., 2012]. This analysis was performed for a 600×600 m area surrounding the GPR-surveyed area and included 2370 trees.

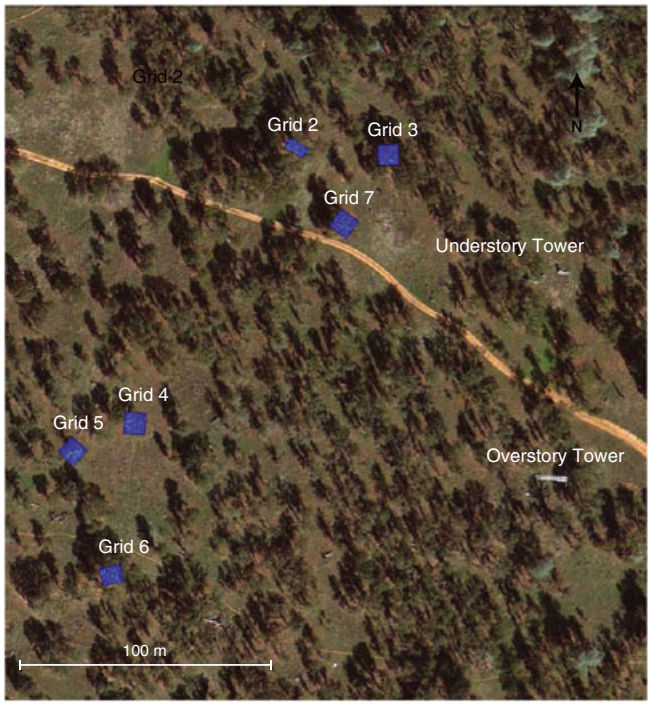

Figure 5. Location of the surveyed grids at (blue rectangles; size is in scale).

3. Results

3.1. GPR Methodology

[22] During measurements, differences in GPR image profiles were apparent between areas below tree canopies, in which distinct hyperbolas interpreted as roots were observed, and open grassy areas in-between trees, for which no or few hyperbolas were detected (Figure 2). We estimated wave velocity for different lines (position) and slices (depth) based on hyperbolas' shape and found a range of values between 0.09 and 0.12 m ns^{-1}, with an average resembling that of the typical velocity for soils (0.10 m ns^{-1}), which was chosen as average and applied to all measurements.

[23] These data were used to produce surface map slices of GPR reflections for each 2.5 cm layer. Despite the applied DME processing routine, noise was still observed in the upper three layers (i.e., to a depth of 7.5 cm; Figure 2). Below these top layers, we identified different elongated elements from the GPR map slices and interpreted them as roots (Figure 6). This interpretation was validated though in situ field sampling for seven individual cases (Figure 7). Validated root samples varied in depth between 8 and 35 cm and in diameter between 13 and 100 mm (roots are indicated and numbered on Figure 6, and their dimensions noted in Table 2).

[24] Depth profiles of GPR reflections showed a distinct peak in values at the bottom of each profile. When compared to excavated bedrock depth, we found that the observed GPR peaks coincided with bedrock depth (Figure 8). We used this finding to determine bedrock depth at our site. However, peak values varied largely and ranged between 4500 to 11,000 mV for different pits. Accordingly, our attempts to define a threshold value indicative of roots, in order to adopt the methodology proposed by *Butnor et al*. [2003], failed: choosing a low reflectance threshold value led to cases in which the soil/bedrock interface was interpreted as root, while choosing a high value inferred some roots might be neglected. Nonetheless, when comparing the excavated dry root biomass in the small pits to the GPR signal obtained by extracting the corresponding area from the larger GPR grid, we observed a good correlation between GPR and pit data. Among the 12 excavated pits (two for each GPR grid), five contained very low root biomass (<450 g), which was below detection. We also eliminated an additional pair of values, which was assumed to have a sampling error. This resulted in a sample size of $n = 6$ pits but high correlation coefficient and significance ($R^2 = 0.90$, $p < 0.05$; Figure 8). Once determined, this relationship was applied to the entire surveyed grid area.

$$\text{Root biomass}\left(\text{kg m}^{-3}\right) = 0.67 \cdot \text{GPR signal (volt)} - 87.07 \quad (1)$$

[25] When analyzing GPR images, we first detected the depth of maximum reflectance for each column of pixels (32 depth slices) and identified the depth where the GPR signal was at its local minimum above this depth. We assumed

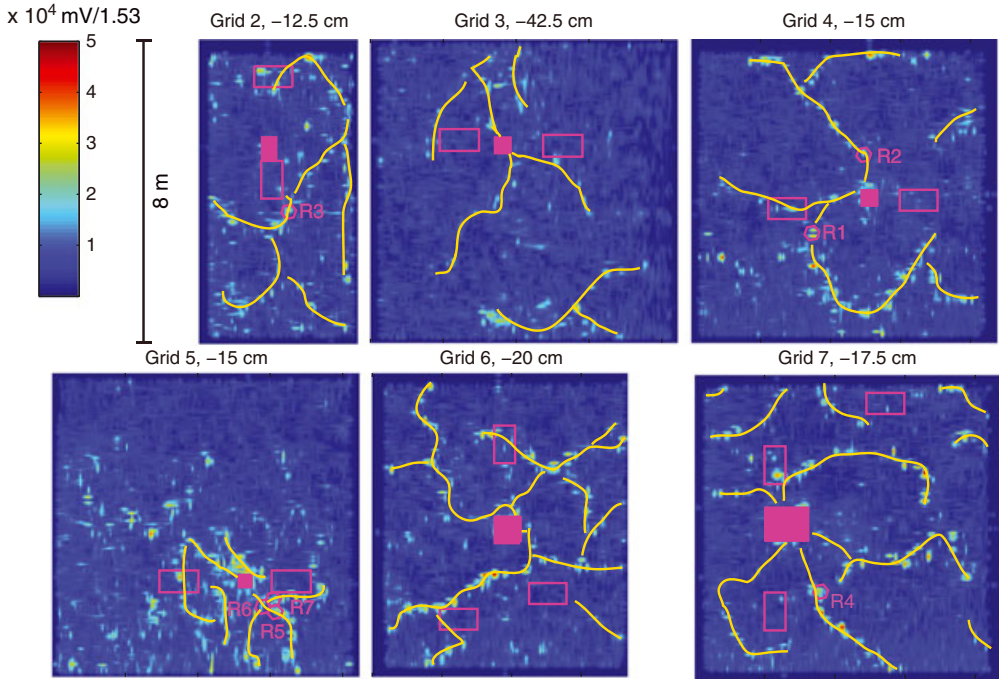

Figure 6. GPR reflection intensity (factory-defined output units are milli-volt/1.56) for each of the surveyed grids. High intensity denotes the existence of roots. The larger roots were digitized to improve their appearance (no change in the values used for calculations). Variations in grid size are a result of field limitations (Table 1). The depth of the specific layer presented is noted above the image. Full rectangles denote the tree bole position. Empty rectangles denote the locations of the excavated pits. Empty polygons denote roots revealed for verification (Table 2 and Figure 7).

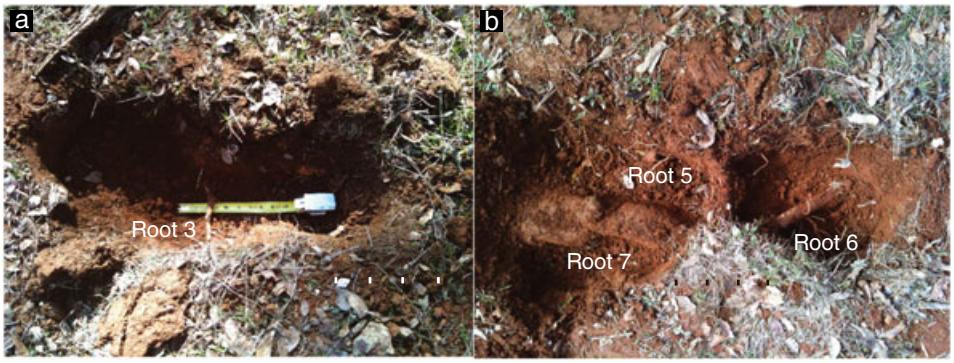

Figure 7. Examples of verified roots. (a) Pit 2; R3. (b) Pit 5; R5, R6, R7. Diameter and depth of roots are presented in Table 2. Note that the excavated pit in Grid 5 was located on the edge of these three large roots (Figure 6), emphasizing the shortcoming of standard sampling methods.

Table 2. Description of the Roots Identified in GPR Images (Figure 6) and Verified In Situ

Root no.	Grid no.	Depth (cm)	Diameter (mm)
1	4	15	25
2	4	12	20
3	2	16	13
4	7	30	38
5	5	12	30
6	5	8	50
7	5	12	100

that this point corresponded with the minimum depth at which bedrock began to affect the GPR signal and used this information to define soil depth for each column. Finally, within the soil profile, GPR reflectance for each data pixel was converted to root biomass according to equation (1), resulting in a three-dimensional representation of root biomass.

3.2. Soil Depth, Coarse Root Biomass, and Root Architecture

[26] Average soil depth was similar for both methods: 37 ± 15 cm for the six 8×8 m GPR grids and 40 ± 17 cm

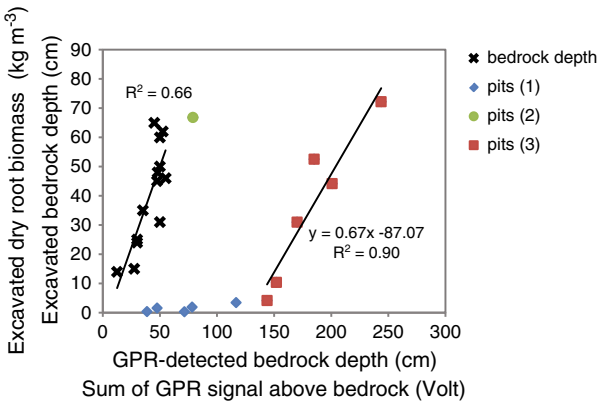

Figure 8. A good fit was found between excavated bedrock depth and bedrock depth detected with GPR (black cross markers). A good fit was also found between excavated dry root biomass and GPR signal intensity for the pits (3) series. Pit series: (1) low root biomass, excluded from calibration, (2) sample error, excluded from calibration, and (3) used for calibrating GPR signal to dry root biomass.

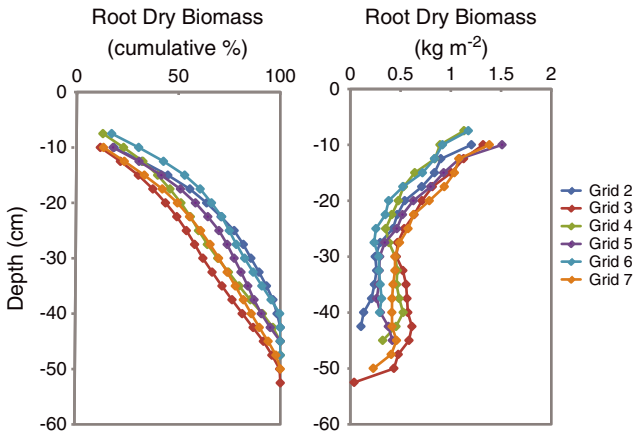

Figure 10. Root biomass with depth as determined with GPR ((right) total values and (left) cumulative values with increasing depth). Coarse root biomass decreased with depth below the topsoil down to 25 cm and increase below that down to 50 cm. The allocation of root biomass deeper in the soil profile was especially evident for the large (old) and isolated trees (Grids 3, 4, and 7).

for the twelve 60 × 100 cm excavated pits (Table 1). Spatial variability in soil depth was high, and bedrock was exposed at depth ranging between 14 and 90 cm. Through GPR images, we observed that these variations occurred over short distances and revealed a complex bedrock topography below the soil (Figure 9). These observations were supported by results from pits, where excavated soil depth varied among neighboring sites.

[27] Root biomass depth profiles obtained from GPR analysis showed a decrease in density from a depth of 10 cm (1–1.5 kg m^{-2}, Figure 10) to 30 cm (~0.5 kg m^{-2}). Below 40 cm, an increase in root density was observed for the large, isolated trees. Depth-biomass profiles were less easy to obtain with the excavation method, but results showed a similar pattern: 33% of biomass was located in the upper 20 cm, 46% between 20 and 50 cm, and 22% below 50 cm (Figure 11). The root biomass found below 50 cm came entirely from two pits, each associated with a different large and isolated tree, in which large roots where detected lying on top of the bedrock. Horizontal profiles of root biomass produced with GPR indicated highest densities around the bole (Figure 12), with only 20% of coarse root biomass observed beyond 2.5 m from the bole, even for larger trees.

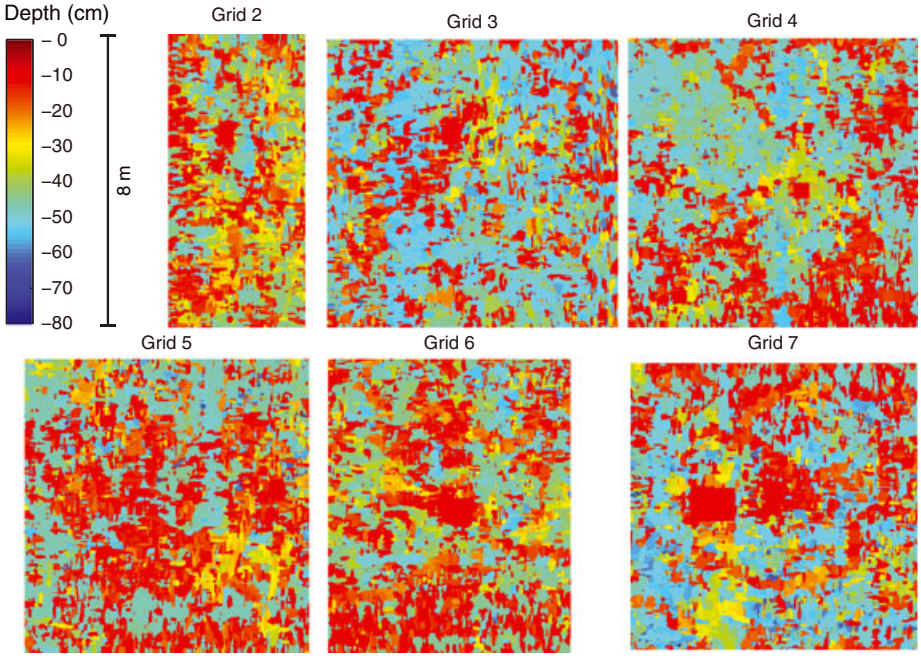

Figure 9. Soil depth interpreted by GPR for each of the surveyed grids. Soil depth showed high spatial variability between grids and even within each tree grid.

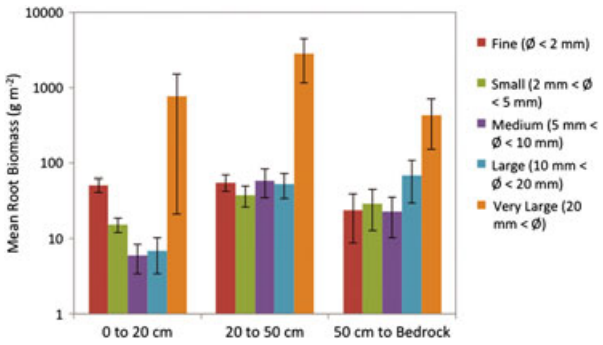

Figure 11. Coarse root biomass (vertical axis, logarithmic scale) average for 15 excavated pits divided into depth categories (horizontal axis) and root class categories (diameter, Ø, varied by color). The highest biomass was observed between depths of 20 to 50 cm, contributed mostly by a few very large roots. Fine root biomass might be underestimated in this study and is better represented for this site in a companion study which relies on soil cores for root biomass estimation. Size class categories follow those designated by Bohm (1979).

[28] Total tree root biomass for the whole 8×8 m grids obtained from GPR analysis varied between 174 kg (tree cluster) and 592 kg (large, isolated tree; Table 1). Root density was lower for the small tree and tree clusters (2–6 kg m^{-2} at a distance of 0.5 m from the bole) and higher for larger trees (10–12 kg m^{-2} for the same distance). Average root biomass based on the six 8×8 m grids was 7.0 ± 2.8 kg m^{-2}. Average root biomass calculated on the basis of the 12 excavated pits was 4.5 kg m^{-2}, with high variability between pits (0.03–21.5 kg m^{-2}).

[29] We used our acquired understanding of the root architecture in this ecosystem to upscale root density. When comparing root density for grids of similar tree size and clumping, deviation between sites was relatively small: root biomass was largest for the three large and isolated trees (10.3 ± 1.3 kg m^{-2}), intermediate for the two tree clusters (6.8 ± 0.2 kg m^{-2}), and smallest for the small tree (4.3 kg m^{-2}). Beyond 4 m from the bole, root densities were low, relatively constant, and similar for all surveyed grids (0.5 ± 0.3 kg m^{-2}). Following field measurements, we developed parameters to sort trees into these three tree configurations based on their dimensions. Observations showed that tree height was similar for large and isolated trees and for clustered trees, but canopy width was roughly twice as large for isolated trees when compared to clustered trees. Small trees were significantly shorter than other trees. We accordingly divided the lidar-based tree population into the three tree configuration categories: 738 stems were of large and isolated trees (canopy height >7.5 m and canopy width >10 m), 1259 stems were of trees growing in clusters (canopy height >7.5 m and canopy width <10 m), and 366 stems were small trees (canopy height <7.5 m). Based on our results, roots were restricted to an area of 4 m radius around the bole for this calculation. Stand-scale root biomass was calculated as follows:

$$\mathrm{RB_{ss}} = \left[\sum_{k=1}^{3} \mathrm{RB}_k \cdot \times N_k \cdot \Pi \cdot r^2 + \mathrm{RB}_4 \cdot \left(S - \sum_{k=1}^{3} N_k \cdot \Pi \cdot r^2\right)\right] / S \quad (2)$$

where $\mathrm{RB_{ss}}$ (kg m^{-2}) is stand-scale root biomass and $\mathrm{RB_k}$ (kg m^{-2}) is the biomass of each tree configuration k: (1) large isolated trees, (2) trees in clusters, (3) small trees, and (4) areas between trees. N is the number of stems in each category within the lidar surveyed area. r is the effective canopy radius (4 m). S is the lidar surveyed area ($3.6 \cdot 10^5$ m^2). Based on this calculation, stand-scale root biomass was 2.8 ± 0.4 kg dry matter m^{-2}.

4. Discussion

4.1. GPR Technology—Capabilities and Limitations

[30] In an ideal system, roots can be easily detected by GPR, based on the large difference in the dielectric permittivity between dry soils and water-conducting roots. However, real ecosystems are more complicated. Site characteristics such as soil texture and water content [*Grote et al.*, 2003; *Huisman et al.*, 2003], root depth, root inclination, and root water content [*Barton and Montagu*, 2004; *Dannoura et al.*, 2008; *Zanetti et al.*, 2010] have a large effect on system performance. Moreover, determining root biomass based on GPR signal is based on the assumed relationships between (a) strong electromagnetic reflection and the existence of a root

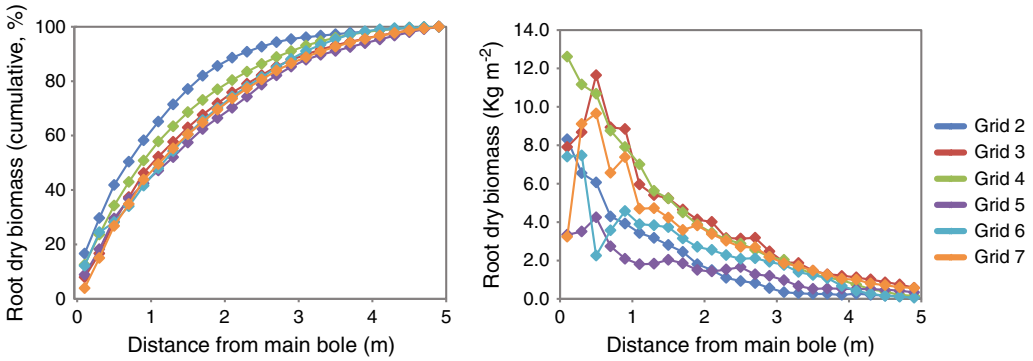

Figure 12. Root biomass with distance from the bole, as determined with GPR ((right) total values and (left) cumulative values with increasing distance). Coarse root biomass decreased rapidly with increasing distance from bole, and was relatively constant after a distance of 4 m. Eighty percent of biomass falls within a distance of 2.5 m from the bole.

surface [*Dannoura et al*., 2008; *Hirano et al*., 2008] and (b) root surface area and root mass [*Dalton*, 1995].

[31] A number of different parameters can be used to transform the GPR signal into root biomass estimates. Through our literature review, it became apparent that different reflectance-related parameters were most closely correlated with root biomass at different field sites. These include time interval of the returning signal [*Barton and Montagu*, 2004], intensity of the reflected wave [*Dannoura et al*., 2008], area of high reflectance within a defined intensity threshold [*Butnor et al*., 2001; *Dannoura et al*., 2008], and number of pixels within the threshold range [*Butnor*, 2003; *Stover et al*., 2007; *Dannoura et al*., 2008]. Although the threshold method (i.e., identifying a reflectance threshold value above which signals are designated as roots) was most widely used, we found it inappropriate for our site. One reason for this may have been the relatively shallow soils at our site, which does not allow for much depth separation. Another reason may be associated with the non-uniformity of root inclination. This complicates root detection due to variations in the interception angle between the root and the GPR antenna, affecting the returning GPR pulse [*Butnor et al*., 2001; *Barton et al*., 2003; *Zenone et al*., 2008]. As an outcome, GPR images of roots often do not look like continuous lineaments (Figure 6). The use of a higher radar frequency (such as 1.5 GHz) with a smaller footprint (approximately 0.5 cm) may have decreased this effect but would have resulted with a shallow penetration depth (most likely less than 20 cm for silt-loam-textured soils such as those at our site). A more dense survey configuration with smaller spacing between lines might have also decreased this effect.

[32] Total GPR reflectance per soil column had the highest correlation with root biomass at our site. Potential bias associated with this particular metric includes misinterpretation of depth and density signals, and interference produced by soil moisture [*Barton and Montagu*, 2004]. However, the degree of bias is likely small: *Stover et al*. [2007] showed that soil moisture affected GPR interpolation only under saturated conditions, and *Cox et al*. [2005] showed that signal strength was more strongly controlled by root diameter than by burial depth. Further, basing our calibration on the complete soil column probably decreased the previously mentioned complications caused by variations in interception angle between the root and GPR antenna. Despite potential errors, field verification of GPR root images was successful, and GPR depth profiles were comparable to those obtained from excavated roots. Moreover, our stand-scale root biomass estimation of 2.8 ± 0.4 kg dry matter m^{-2} was similar to previous estimates based on allometric relationships for this field site: 1.2 kg C m^{-2} or approximately 2.4 kg m^{-2} of dry root biomass [*Baldocchi et al*., 2010].

[33] The ability of GPR to survey large areas, and thus account for the large spatial variability of tree roots, speaks to its superiority over pit excavation methods alone. Comparison with the excavation method emphasized the shortcoming of standard excavation sampling, which often miss root clusters. For example, in Figure 7b, a cluster of very large and shallow roots was observed by GPR and later verified in situ, but root biomass from an excavated pit selected prior to the GPR survey and randomly located on the edge of these roots indicated very low coarse root biomass associated with this tree. Another advantage of GPR is the ability to estimate biomass of very large roots, which cannot be excavated.

[34] Despite assumptions, complexities, and limitations involved with GPR root survey, our research shows that when a careful site-specific calibration procedure is followed, GPR technology can successfully visualize and quantify coarse tree roots over large areas, therefore accounting for their large spatial heterogeneity.

4.2. Soil Depth, Coarse Root Biomass, and Root Architecture

[35] Soils serve as a reservoir for water, and therefore, the depth of this medium is an important factor in plant water availability. At our research site, soil depth was found to vary largely but was skewed towards more shallow depths, and roots were observed throughout the whole soil profile.

[36] Total tree root biomass varied between the six sampled trees and was lower for the small tree and tree clusters, and higher for the large and isolated trees (Table 1). Root biomass was expected to be low for the small tree (260 kg, Grid 5). Low root biomass for trees growing in clusters (174 kg, Grid 2 and 350 kg, Grid 6) was supported by the lidar-based imagery analysis, which showed that canopy width of trees growing in clusters was considerably smaller than that of the isolated trees of similar height and probably lower aboveground biomass. Amongst the large trees, the largest and oldest tree (521 kg, Grid 7) did not support the largest root biomass (592 kg, Grid 3). An attempt to age this old tree with an increment borer was unsuccessful, because most of the bole was hollow. Our root biomass estimate indicates that a similar process of coarse root decay may also take place belowground.

[37] Combining GPR and lidar analysis to upscale tree root biomass to stand-scale biomass resulted in an estimate of 2.8 ± 0.4 kg dry matter m^{-2}, which is similar to previous estimates based on allometric relationships for this field site [*Baldocchi et al*., 2010]. In the quoted research, aboveground biomass was estimated to be 7.4 kg dry matter m^{-2}, producing a 2.6:1 relationship between aboveground and belowground biomass.

[38] GPR-based mapping of root distribution showed that for larger and older trees, an increase in root density was detected above the bedrock. Presumably, root proliferation just above the bedrock occurs as a result of lateral growth on the bedrock surface when roots meet boundary of reduced permeability. Because percolating soil water will be stopped at the bedrock, this interface creates a desired environment for roots. More so, such rooting pattern may indicate on root penetration through the soil/bedrock interface.

[39] Lateral coarse root distribution was found to be limited to a short distance from the bole, creating large heterogeneity in lateral coarse root density between trees and open grassland patches. Only 20% of coarse root biomass was observed beyond 2.5 m from the bole, even for larger trees. Interestingly, these results provided additional verification for previous research at this site, which found that soil respiration decreased with distance from the tree bole, dropping off beyond a distance of 2–3 m [*Tang and Baldocchi*, 2005]. These findings differ from those of temperate and semi-arid sites, which more often report finding shallow root systems that extend to much greater distances laterally [*Rutherford*, 1983; *Mordelet et al*., 1997; *Macinnis-Ng et al*., 2010; *Litvak et al*., 2011], in order to efficiently capture the shallow soil

water. Instead, the root architecture at this site appears more typical of the deep and narrow root systems at arid sites [*Akpo*, 1993; *Hipondoka et al*., 2003].

[40] Why, then, are not coarse root architecture in this ecosystem more similar to those of other semi-arid ecosystems? We explain this rooting pattern by the linkage between tree phenology and soil water availability, as follows. At this site, oaks leaf out during early spring warming, when soil water content is at its peak ($>30\%$ m^3 m^{-3}). Ecosystem CO_2 uptake reaches peak flux rates in June, and at this time, water content is still abundant ($>20\%$ m^3 m^{-3}, Figure 3). Therefore, in most years, the ecosystem is energy limited and not water limited throughout the growing season, eliminating the need for an extensive coarse lateral root system, which would exceed that required to meet peak demands. However, a concurrent study at this site indicates that fine roots, which can be highly ephemeral, extend to much greater distances laterally at the time of peak growth and thereby facilitate water uptake while water is abundant [*Koteen et al*., in prep.]. Secession of the rain season in late May occurs when temperatures are already warm and further accelerate soil drying, so that within a short period, soil moisture drops from above 20% in June to below 10% in July (Figure 3). In summer, drought conditions are extreme, even for Mediterranean-type vegetation, and pre-dawn water potentials as low as -6 MPa have been measured [*Baldocchi et al*., 2004]. Therefore, maintaining an extensive coarse lateral root system during the dry season would impose significant metabolic costs at a time of high stress and when soils are too depleted in soil moisture for significant root water uptake.

[41] Both aboveground and belowground dynamics reflect adaptation to constraints imposed by the intense seasonality of the Mediterranean-type climate and exhibit characteristic strategies. Aboveground, oaks have been shown to enhance stomatal closure and to down-regulate photosynthetic functions (i.e., maximum carboxylation rates (Vc_{max}) and the rate of light saturated photosynthetic electron transport (J_{max})). These adjustments allow them to restrict water loss while maintaining low rates of productivity [*Dickson and Tomlinson*, 1996; *Vaz et al*., 2010]. Belowground, the narrow root architecture most likely enhances water uptake from groundwater during the dry season by roots that penetrate the bedrock. In addition to summer groundwater uptake which has been verified for this site [*Miller et al*., 2010], we speculate that two other processes associated with deep water sources may improve water uptake during the dry season: water uptake from fissures in the bedrock itself [*Stone and Kalisz*, 1991; *Schiller et al*., 2010; *Schwinning*, 2010] and hydraulic lift from deeper soil layers and bedrock fissures to the fine roots located at shallower depths [*Ishikawa and Bledsoe*, 2000; *Prieto et al*., 2012].

5. Conclusion

[42] The binary nature of this Mediterranean savanna, in which water is either abundantly available or scarce, is reflected in the architecture of the tree root system. The explicit tradeoff between investment in an extensive root system to capture water when it is abundant, and the need to maintain that system when water is scarce, is revealed in a root system that is narrow and deep.

[43] These findings were obtained by surveying coarse tree roots with ground penetrating radar. The feasibility of GPR to determine soil depth, map coarse roots, and estimate their biomass was tested and found successful. Calibration of GPR signals against manual sampling of roots in excavated pits allowed us to estimate root biomass and to produce a three-dimensional characterization of coarse roots in this ecosystem. Measurements from this survey have shown that soils are relatively shallow and that tree roots extensively occupy the whole soil profile, with large trees exhibiting a peak in biomass at the bottom of the soil profile. The radial extension of roots was found to be small—density decreased with distance from the bole and dropped sharply at a distance shorter than the drip line.

[44] In order to upscale these measurements to the landscape scale, we used lidar data of tree distribution and architecture. We calculated the relative abundance of each tree size and type (isolated versus clusters of trees) from the lidar data and used scaling relationships to upscale our GPR measurements. The sum of the stand-scale root biomass (2.8 ± 0.4 kg dry matter m^{-2}) matched independent estimates that were derived from earlier-determined forest allometric relationships.

[45] In this research, we have characterized the distribution of coarse tree roots of a North-Californian oak savanna in order to better understand the ecohydrology of this system. We have found that from an ecohydrological point of view, a narrow and deep tree coarse root system is more practical for this oak savanna both during the water abundant growing season and the water depleted carbohydrate maintenance season. Such information is important for future assessment of ecosystem sensitivity to changes, especially in groundwater recharge originating from the Sierra Nevada snow cover; changes in annual precipitation amounts, storm intensity, and temporal distribution of storms over the course of the year; and regeneration of new seedlings. Our research has shown that the combination of resource availability, which is primarily water in this ecosystem, and plant demand is portrayed in the form of the root system.

[46] **Acknowledgment.** This research was supported by Vaadia-BARD Postdoctoral Fellowship Award No. FI-429-2009 from BARD, the United States—Israel Binational Agricultural Research and Development Fund. The research site was funded by the US Department of Energy Grant DE-SC0005130. We thank Tomi Kaplan and Sergey Vichik for their help in data analyzing. We thank Russell Tonzi for use of his ranch. We thank Joe Verfaillie, Siyan Ma, Hanna Buechi, and Ofer Raz for help in the field and lab.

Bibliography

Adrian, N. (2004), Ground-penetrating radar and its use in sedimentology: principles, problems and progress, *Earth-Science Reviews*, *66*(3-4), 261–330, doi:10.1016/j.earscirev.2004.01.004.

Akpo, E. (1993), *Influence du couvert ligneux sur la structure et le fonctionnement de la strate herbacée en milieu sahélien*, ORSTOM, Paris.

Baldocchi, D. D., L. K. Xu, and N. Kiang (2004), How plant functional-type, weather, seasonal drought, and soil physical properties alter water and energy fluxes of an oak-grass savanna and an annual grassland, *Agric. For. Meteorol.*, *123*(1-2), 13–39, doi:10.1016/j.agrformet.2003.11.006.

Baldocchi, D. D., Q. Chen, X. Chen, S. Ma, G. R. Miller, Y. Ryu, J. Xiao, R. Wenk, and J. Battles (2010), The dynamics of energy, water, and carbon fluxes in a blue oak (*Quercus douglasii*) savanna in California, in *Ecosystem Function in Savannas*, pp. 135–154, CRC Press, Boca Raton, Fla.

Barton, C. V. M., and K. D. Montagu (2004), Detection of tree roots and determination of root diameters by ground penetrating radar under optimal conditions, *Tree Physiology*, *24*(12), 1323–1331, doi:10.1093/treephys/24.12.1323.

Bohm, W. (1979), *Methods of Studying Root Systems / Wolfgang Bohm*, Ecological Studies; v. *33*, Springer-Verlag, Berlin; New York:

Butnor, J. (2003), Symposium: Approaches and technologies for detecting changes in forest soil carbon pools—Utility of Ground-penetrating radar as a root biomass survey tool in forest systems., *Soil Science Society of America journal*., *67*(5), 1607.

Butnor, J. R., J. A. Doolittle, L. Kress, S. Cohen, and K. H. Johnsen (2001), Use of ground-penetrating radar to study tree roots in the southeastern United States, *Tree Physiology*, *21*(17), 1269–1278, doi:10.1093/treephys/21.17.1269.

Butnor, J. R., J. A. Doolittle, K. H. Johnsen, L. Samuelson, T. Stokes, and L. Kress (2003), Utility of Ground-Penetrating Radar as a Root Biomass Survey Tool in Forest Systems, *Soil Sci. Soc. Am. J.*, *67*(5), 1607, doi:doi:10.2136/sssaj2003.1607.

Canadell, J., R. B. Jackson, J. R. Ehleringer, H. A. Mooney, O. E. Sala, and E. D. Schulze (1996), Maximum rooting depth of vegetation types at the global scale, *Oecologia*, *108*(4), 583–595, doi:10.1007/BF00329030.

Chamberlain, A. T., W. Sellers, C. Proctor, and R. Coard (2000), Cave detection in limestone using ground penetrating radar, *Journal of Archaeological Science*, *27*(10), 957–964, doi:10.1006/jasc.1999.0525.

Chen, Q., D. Baldocchi, P. Gong, and T. Dawson (2008), Modeling radiation and photosynthesis of a heterogeneous savanna woodland landscape with a hierarchy of model complexities, *Agric. For. Meteorol.*, *148*(6-7), 1005–1020, doi:10.1016/j.agrformet.2008.01.020.

Cheng, X. M., and C. S. Bledsoe (2002), Contrasting seasonal patterns of fine root production for blue oaks (*Quercus douglasii*) and annual grasses in California oak woodland, *Plant Soil*, *240*(2), 263–274, doi:10.1023/A:1015723314433.

Coomes, D. A., and P. J. Grubb (2000), Impacts of root competition in forests and woodlands: A theoretical framework and review of experiments, *Ecol. Monogr.*, *70*(2), 171–207, doi:10.1890/0012-9615(2000)070[0171:IORCIF]2.0.CO;2.

Cox, K. D., H. Scherm, and N. Serman (2005), Ground-penetrating radar to detect and quantify residual root fragments following peach orchard clearing, *HortTechnology*, *15*(3), 600–607.

Daniels, D. J. (1996), Surface-penetrating radar, *Electron. Commun. Eng. J.*, *8*(4), 165–182, doi:10.1049/ecej:19960402.

Dalton, F. N. (1995), In-situ root extent measurements by electrical capacitance methods, *Plant and soil*, *173*(1), 157–165.

Dannoura, M., Y. Hirano, T. Igarashi, M. Ishii, K. Aono, K. Yamase, and Y. Kanazawa (2008), Detection of *Cryptomeria japonica* roots with ground penetrating radar, *Plant Biosystems—An International Journal Dealing with all Aspects of Plant Biology*, *142*, 375–380, doi:10.1080/11263500802150951.

Day, F. P., E. P. Weber, C. R. Hinkle, and B. G. Drake (1996), Effects of elevated atmospheric CO2 on fine root length and distribution in an oak-palmetto scrub ecosystem in central Florida, *Glob. Change Biol.*, *2*(2), 143–148, doi:10.1111/j.1365-2486.1996.tb00059.x.

Dickson, R. E., and P. T. Tomlinson (1996), Oak growth, development and carbon metabolism in response to water stress, *Annales des Sciences Forestières*, *53*(2-3), 16, doi:10.1051/forest:19960202.

Drexhage, M., M. Chauviere, F. Colin, and C. Nielsen (1999), Development of structural root architecture and allometry of *Quercus petraea*, *Can. J. For. Res.-Rev. Can. Rech. For.*, *29*(5), 600–608, doi:10.1139/cjfr-29-5-600.

Fogel (1983), Root turnover and productivity of coniferous forests, *Plant and Soil*, *71*(1–3), 75–85, doi:10.1007/BF02182643.

Fourcaud, T., J. Hruska, J. Cermak, V. Nadyezhdin, and L. Praus (2002), An evaluation of different methods to investigate root system architecture of urban trees in situ: I. Ground-penetrating radar, *Architecture*, *28*(1), 2–10.

Grote, K., S. Hubbard, and Y. Rubin (2003), Field-scale estimation of volumetric water content using ground-penetrating radar ground wave techniques, *Water Resour. Res.*, *39*(11), doi:10.1029/2003WR002045.

Guswa, A. J. (2008), The influence of climate on root depth: A carbon cost-benefit analysis, *Water Resour. Res.*, *44*(2), doi:10.1029/2007WR006384.

Heisler-White, J. L., A. K. Knapp, and E. F. Kelly (2008), Increasing precipitation event size increases aboveground net primary productivity in a semi-arid grassland, *Oecologia*, *158*(1), 129–140, doi:10.1007/s00442-008-1116-9.

Hipondoka, M. H. T., J. N. Aranibar, C. Chirara, M. Lihavha, and S. A. Macko (2003), Vertical distribution of grass and tree roots in arid ecosystems of Southern Africa: Niche differentiation or competition?, *J. Arid. Environ.*, *54*(2), 319–325, doi:10.1006/jare.2002.1093.

Hirano, Y., M. Dannoura, K. Aono, T. Igarashi, M. Ishii, K. Yamase, N. Makita, and Y. Kanazawa (2008), Limiting factors in the detection of tree roots using ground-penetrating radar, *Plant and Soil*, *319*, 15–24, doi:10.1007/s11104-008-9845-4.

Hruska, J., J. Cermak, and S. Sustek (1999), Mapping tree root systems with ground-penetrating radar., *Tree Physiology*, *19*(2), 125–130.

Huisman, J. A., S. S. Hubbard, J. D. Redman, and A. P. Annan (2003), Measuring soil water content with ground penetrating radar: A review, *Vadose Zone Journal*, *2*(4), 476–491, doi:10.2113/2.4.476.

Ishikawa, C. M., and C. S. Bledsoe (2000), Seasonal and diurnal patterns of soil water potential in the rhizosphere of blue oaks: Evidence for hydraulic lift, *Oecologia*, *125*(4), 459–465.

Jackson, R. B., J. Canadell, J. R. Ehleringer, H. A. Mooney, O. E. Sala, and E. D. Schulze (1996), A global analysis of root distributions for terrestrial biomes, *Oecologia*, *108*(3), 389–411, doi:10.1007/BF00333714.

Jones, S. B., J. M. Wraith, and D. Or (2002), Time domain reflectometry measurement principles and applications, *Hydrological Processes*, *16*(1), 141–153, doi:10.1002/hyp.513.

Kleidon, A., and M. Heimann (1998), Optimised rooting depth and its impacts on the simulated climate of an atmospheric general circulation model, *Geophys. Res. Lett.*, *25*(3), 345–348, doi:10.1029/98GL00034.

Knapp, A. K. *et al.* (2008), Consequences of more extreme precipitation regimes for terrestrial ecosystems, *Bioscience*, *58*(9), 811–821, doi:10.1641/B580908.

Kobayashi, H., D. D. Baldocchi, Y. Ryu, Q. Chen, S. Ma, J. L. Osuna, and S. L. Ustin (2012), Modeling energy and carbon fluxes in a heterogeneous oak woodland: A three-dimensional approach, *Agric. For. Meteorol.*, *152*, 83–100, doi:10.1016/j.agrformet.2011.09.008.

Kramer, P. J. (1969), *Plant and Soil Water Relationships: A Modern Synthesis*, McGraw-Hill Book Company, New York, USA

Lewis, D. C., and R. H. Burgy (1964), The relationship between oak tree roots and groundwater in fractured rock as determined by tritium tracing, *Journal of Geophysical Research*, *69*(12), 2579–2588, doi:10.1029/JZ069i012p02579.

Litvak, M., S. Schwinning, and J. Heilman (2011), Woody plant rooting depth and ecosystem function of savannas: A case study from the Edwards Plateau Karst, Texas, in Ecosystem Function in Savannas, pp. 117–134, CRC Press.

Lorenzo, H., V. Perez-Gracia, A. Novo, and J. Armesto (2010), Forestry applications of ground-penetrating radar, *For. Syst.*, *19*(1), 5–17.

Lynch, J. (1995), Root architecture and plant productivity, *Plant Physiol.*, *109*(1), 7–13.

Ma, S., D. D. Baldocchi, L. Xu, and T. Hehn (2007), Inter-annual variability in carbon dioxide exchange of an oak/grass savanna and open grassland in California, *Agric. For. Meteorol.*, *147*(3–4), 157–171, doi:10.1016/j.agrformet.2007.07.008.

Macinnis-Ng, C. M. O., S. Fuentes, A. P. O'Grady, A. R. Palmer, D. Taylor, R. J. Whitley, I. Yunusa, M. J. B. Zeppel, and D. Eamus (2010), Root biomass distribution and soil properties of an open woodland on a duplex soil, *Plant Soil*, *327*(1-2), 377–388, doi:10.1007/s11104-009-0061-7.

Makela, A., H. T. Valentine, and H.-S. Helmisaari (2008), Optimal co-allocation of carbon and nitrogen in a forest stand at steady state, *New Phytol.*, *180*(1), 114–123, doi:10.1111/j.1469-8137.2008.02558.x.

Miller, G. R., X. Chen, Y. Rubin, S. Ma, and D. D. Baldocchi (2010), Groundwater uptake by woody vegetation in a semiarid oak savanna, *Water Resour. Res.*, *46*, doi:10.1029/2009WR008902.

Millikin, C. S., and C. S. Bledsoe (1999), Biomass and distribution of fine and coarse roots from blue oak (*Quercus douglasii*) trees in the northern Sierra Nevada foothills of California, *Plant Soil*, *214*(1-2), 27–38.

Mordelet, P., J. Menaut, and A. Mariotti (1997), Tree and grass rooting patterns in an African humid savanna, *Journal of Vegetation Science*, *8*(1), 65–70, doi:10.2307/3237243.

Olhoeft, G. R. (2002), Applications and frustrations in using ground penetrating radar, *IEEE Aerospace and Electronic Systems Magazine*, *17*(2), 12–20, doi:10.1109/62.987130.

Park, B. R., R. D. Yanai, M. A. Vadeboncoeur, and S. P. Hamburg (2007), Estimating root biomass in rocky soils using pits, cores, and allometric equations, *Soil Sci. Soc. Am. J.*, *71*(1), 206–213, doi:10.2136/sssaj2005.0329.

Pérez Gracia, V., J. A. Canas, L. G. Pujades, J. Clapés, O. Caselles, F. Garcia, and R. Osorio (2000), GPR survey to confirm the location of ancient structures under the Valencian Cathedral (Spain), *Journal of Applied Geophysics*, *43*(2-4), 167–174, doi:10.1016/S0926-9851(99)00056-7.

Prieto, I., C. Armas, and F. I. Pugnaire (2012), Water release through plant roots: New insights into its consequences at the plant and ecosystem level, *New Phytol.*, *193*(4), 830–841, doi:10.1111/j.1469-8137.2011.04039.x.

Robinson, D. A., S. B. Jones, J. M. Wraith, D. Or, and S. P. Friedman (2003), A review of advances in dielectric and electrical conductivity measurement in soils using time domain reflectometry, *Vadose Zone Journal*, *2*(4), 444–475, doi:10.2113/2.4.444.

Rutherford, M. (1983), Growth-rates, biomass and distribution of selected woody plant roots in Burkea africana-Ochna pulchra savanna, *Vegetatio*, *52*(1), 45–63.

Sala, O., W. Lauenroth, and C. Reid (1982), Water relations—A new dimension for niche separation between *Bouteloua gracilis* and *Agropyron smithii* in North-American semi-arid grasslands, *J. Appl. Ecol.*, *19*(2), 647–657, doi:10.2307/2403496.

Schenk, H. J., and R. B. Jackson (2002), Rooting depths, lateral root spreads and below-ground/above-ground allometries of plants in water-limited ecosystems, *J. Ecol.*, *90*(3), 480–494, doi:10.1046/j.1365-2745.2002.00682.x.

Schiller, G., E. D. Ungar, S. Cohen, and N. Herr (2010), Water use by Tabor and Kermes oaks growing in their respective habitats in the Lower Galilee region of Israel, *For. Ecol. Manage.*, *259*(5), 1018–1024, doi:10.1016/j.foreco.2009.12.008.

Schultz, J. J., M. E. Collins, and A. B. Falsetti (2006), Sequential monitoring of burials containing large pig cadavers using ground-penetrating radar, *Journal of Forensic Sciences*, *51*(3), 607–616, doi:10.1111/j.1556-4029.2006.00129.x.

Schwinning, S. (2010), The ecohydrology of roots in rocks, *Ecohydrology*, *3*(2), 238–245, doi:10.1002/eco.134.

Stern, W. (1929), Versuch einer elektrodynamischen Dickenmessung von Gletschereis, *German Beitrage zur Geophysik*, *23*, 292–333.

Stone, E., and P. Kalisz (1991), On the maximum extent of tree roots, *For. Ecol. Manage.*, *46*(1-2), 59–102, doi:10.1016/0378-1127(91)90245-Q.

Stover, D. B., F. P. Day, J. R. Butnor, and B. G. Drake (2007), Effect of elevated CO2 on coarse-root biomass in Florida scrub detected by ground-penetrating radar, *Ecology*, *88*, 1328–1334, doi:10.1890/06-0989.

Tang, J. W., and D. D. Baldocchi (2005), Spatial-temporal variation in soil respiration in an oak-grass savanna ecosystem in California and its partitioning into autotrophic and heterotrophic components, *Biogeochemistry*, *73*(1), 183–207, doi:10.1007/s10533-004-5889-6.

Thomas, F. M., and G. Hartmann (1998), Tree rooting patterns and soil water relations of healthy and damaged stands of mature oak (*Quercus robur* L and *Quercus petraea* [Matt] Liebl), *Plant Soil*, *203*(1), 145–158, doi:10.1023/A:1004305410905.

Tyler, C. M., B. Kuhn, and F. W. Davis (2006), Demography and recruitment limitations of three oak species in California, *Q. Rev. Biol.*, *81*(2), 127–152, doi:10.1086/506025.

Vaughan, D. G., H. F. J. Corr, C. S. M. Doake, and E. D. Waddington (1999), Distortion of isochronous layers in ice revealed by ground-penetrating radar, *Nature*, *398*(6725), 323–326, doi:10.1038/18653.

Vaz, M., J. S. Pereira, L. C. Gazarini, T. S. David, J. S. David, A. Rodrigues, J. Maroco, and M. M. Chaves (2010), Drought-induced photosynthetic inhibition and autumn recovery in two Mediterranean oak species (*Quercus ilex* and *Quercus suber*), *Tree Physiol.*, *30*(8), 946–956, doi:10.1093/treephys/tpq044.

Velten, K., and O. Richter (1995), Optimal root/shoot-partitioning of carbohydrates in plants, *Bull. Math. Biol.*, *57*(1), 99–107, doi:10.1016/0092-8240(94)00026-9.

Vogt, K. A., D. J. Vogt, P. A. Palmiotto, P. Boon, J. OHara, and H. Asbjornsen (1996), Review of root dynamics in forest ecosystems grouped by climate, climatic forest type and species, *Plant Soil*, *187*(2), 159–219.

Yanai, R. D., B. B. Park, and S. P. Hamburg (2006), The vertical and horizontal distribution of roots in northern hardwood stands of varying age, *Can. J. For. Res.-Rev. Can. Rech. For.*, *36*(2), 450–459, doi:10.1139/X05-254.

Yaseef, N. R., D. Yakir, E. Rotenberg, G. Schiller, and S. Cohen (2010), Ecohydrology of a semi-arid forest: Partitioning among water balance components and its implications for predicted precipitation changes, *Ecohydrology*, *3*(2), 143–154, doi:10.1002/eco.65.

Yoshikawa, K., and L. D. Hinzman (2003), Shrinking thermokarst ponds and groundwater dynamics in discontinuous permafrost near council, Alaska, *Permafrost and Periglacial Processes*, *14*(2), 151–160, doi:10.1002/ppp.451.

Zanetti, C., A. Weller, M. Vennetier, and P. Mériaux (2010), Detection of buried tree root samples by using geoelectrical measurements: A laboratory experiment, *Plant and Soil*, *339*, 273–283, doi:10.1007/s11104-010-0574-0.

Zenone, T., G. Morelli, M. Teobaldelli, F. Fischanger, M. Matteucci, M. Sordini, A. Armani, C. Ferrè, T. Chiti, and G. Seufert (2008), Preliminary use of ground-penetrating radar and electrical resistivity tomography to study tree roots in pine forests and poplar plantations, *Funct. Plant Biol.*, *35*(10), 1047–1058.